PFC/JA-93-29

Properties of the Kapchinskij-Vladimirskij Equilibrium and Envelope Equation for an Intense Charged-Particle Beam in a Periodic Focusing Field

C. Chen and R.C. Davidson

November, 1993

Plasma Fusion Center
Massachusetts Institute of Technology
Cambridge, MA 02139
and
Plasma Physics Laboratory
Princeton University
Princeton, New Jersey 08543

Submitted for publication in Physical Review E. This work was supported in part by the Office of Naval Research and in part by the Department of Energy High Energy Physics Division.

PROPERTIES OF THE KAPCHINSKIJ-VLADIMIRSKIJ EQUILIBRIUM AND ENVELOPE EQUATION FOR AN INTENSE CHARGED-PARTICLE BEAM IN A PERIODIC FOCUSING FIELD

Chiping Chen
Plasma Fusion Center
Massachusetts Institute of Technology
Cambridge, Massachusetts 02139

Ronald C. Davidson
Plasma Physics Laboratory
Princeton University
Princeton, New Jersey 08543

ABSTRACT

The properties of the Kapchinskij-Vladimirskij (K-V) equilibrium and envelope equation are examined for an intense charged-particle beam propagating through an applied periodic solenoidal focusing magnetic field including the effects of the self-electric and self-magnetic fields associated with the beam space-charge and current. It is found that the beam emittance is proportional to the maximum canonical angular momentum achieved by the particles within the K-V distribution. The Poincaré mapping technique is used to determine systematically the axial dependence of the radius of the matched (equilibrium) beam and to explore nonlinear resonances in the nonequilibrium beam envelope oscillations. Certain correlations are found between the nonlinear resonances and well-known instabilities for the K-V equilibrium. It is shown, for the first time, that the nonequilibrium beam envelope oscillations exhibit chaotic behavior for periodic focusing magnetic fields and sufficiently high beam densities, and that there exists a uniquely matched beam in the parameter regime of practical interest, i.e., $\sigma_0 < 90°$, where σ_0 is the phase advance over one axial period of the focusing field in the absence of space-charge effects. The nonlinear resonances and chaotic behavior in the nonequilibrium beam envelope oscillations may play an important role in mismatched or multiple beam transport, including emittance growth and beam halo formation and evolution.

PACS numbers: 07.77.+p, 29.27.Eg, 41.75.-i, 52.25.Wz

I. INTRODUCTION

The exploration of equilibrium and nonequilibrium properties of an intense charged-particle beam in a periodic focusing channel has been emphasized in high-current accelerator and charged-particle beam research [1, 2]. Such research is critical to the advancement of basic particle accelerator physics and to the design of high-current linear accelerators and high-current beam transport systems. An important application of high-current charged-particle beams is heavy ion fusion [3].

In 1959, Kapchinskij and Vladimirskij [4] constructed the first and only known equilibrium distribution function for a continuous beam in a periodic focusing channel including the effects of beam space-charge and current. This pioneering work has led to theoretical and experimental investigations of several critical aspects of an intense beam focused by a periodic transport channel, including: (i) introduction of the concept of root-mean-squared (rms) emittance [5]-[7], (ii) derivation of the rms beam envelope equations [5, 6, 8], (iii) investigation of current intensity limits [9], (iv) analysis of the stability properties of the Kapchinskij-Vladimirskij equilibrium [10], (v) study of the phenomenon of emittance growth [11]-[15], and (vi) exploration of beam halo formation and evolution [16]. Despite these efforts, a *basic* understanding of the physics of intense charged-particle beam propagation in periodic focusing channels has not yet emerged.

The purpose of this paper is to examine the basic properties of the Kapchinskij-Vladimirskij (K-V) equilibrium and envelope equation for intense charged-particle beam propagation through a periodic solenoidal focusing magnetic field, including the effects of the self-electric and self-magnetic fields associated with beam space charge and current. The K-V equilibrium distribution function is derived. It is emphasized that the periodic solenoidal magnetic field configuration possesses a higher degree of symmetry than the alternating-gradient quadrupole magnetic field configuration. It is shown that the unnormalized emittance determines the upper and lower bounds on the canonical angular

momentum of the particles within the K-V distribution. A normalized beam envelope equation is presented, and it is characterized by two parameters, namely, the intensity of the focusing field and the beam self-field perveance. The properties of the beam envelope equation are examined over a wide region of parameter space. The *Poincaré mapping technique* [17] is used to determine systematically the axial dependence of the radius of the matched (equilibrium) beam and to explore nonlinear resonances in the phase space described by the beam envelope equation. Certain correlations are found between the nonlinear resonances in the nonequilibrium beam envelope oscillations and well-known instabilities [10] for the K-V equilibrium. It is shown, for a periodic focusing magnetic field and sufficiently high beam density, that the nonequilibrium beam envelope oscillations can exhibit *chaotic behavior*, i.e., *a very sensitive dependence on initial conditions.* The nonlinear resonances and chaotic beam envelope oscillations may play an important role in mismatched or multiple beam transport including emittance growth and beam halo formation and evolution. Furthermore, it is shown that there exists a uniquely matched beam in the parameter regime of practical interest, i.e., in the regime where the strong, second-order (envelope) instability [10] is avoided.

The organization of this paper is as follows. In Sec. II, the Hamilton equations of motion are presented for a single particle in both the laboratory frame and the Larmor frame in the paraxial approximation. In Sec. III, the Kapchinskij-Vladimirskij equilibrium distribution function is constructed, and the beam envelope equation is derived. It is shown that the unnormalized emittance determines the upper and lower bounds on the canonical angular momentum of the particles within the K-V distribution. In Sec. IV, the properties of the beam envelope equation are studied using the Poincaré map. The axial dependence of the radius of the matched (equilibrium) beam is obtained and shown to be unique in the parameter regime of practical interest. Chaotic beam envelope oscillations are found for a periodic focusing magnetic field and sufficiently high beam density.

II. CANONICAL DESCRIPTION OF SINGLE-PARTICLE MOTION

In this section, we present a canonical description of the motion of a single particle in an applied periodic solenoidal focusing magnetic field and the equilibrium self-electric and self-magnetic fields associated with an intense nonneutral charged-particle beam. After making the paraxial approximation, we express the Hamiltonian and the equations of motion for a single particle in both the laboratory frame and the time-dependent Larmor frame.

A. Equations of Motion in the Laboratory Frame

We consider an intense charged-particle beam propagating with average axial velocity $\beta_b c\vec{e}_z$ through an applied periodic solenoidal magnetic field described by [1]

$$\vec{B}^{(\mathrm{ext})}(x,y,s) = B_z(s)\vec{e}_z - \frac{1}{2}B_z'(s)(x\vec{e}_x + y\vec{e}_y) \tag{1}$$

in the thin-beam approximation. In Eq. (1), use has been made of the convention $s = z$ to denote axial coordinate, the "prime" denotes derivative with respect to s, and c is the speed of light *in vacuuo*. For a periodic solenoidal magnetic field with the fundamental periodicity length S, the axial magnetic field $B_z(s)$ satisfies the condition

$$B_z(s+S) = B_z(s)\ . \tag{2}$$

The vector potential for the applied magnetic field can be chosen as

$$\vec{A}^{(\mathrm{ext})}(x,y,s) = \frac{1}{2}B_z(s)(-y\vec{e}_x + x\vec{e}_y) \tag{3}$$

with $\vec{B}^{(\mathrm{ext})} = \nabla \times \vec{A}^{(\mathrm{ext})}$.

In the paraxial approximation [1], the transverse particle motion is assumed to be nonrelativistic, and the Budker parameter is small compared with unity, i.e,

$$\nu = q^2 N/mc^2 \ll 1\ , \tag{4}$$

where $N = \int dxdyn_0(x,y,s)$ is the number of particles per unit axial length of the beam, and q and m are the particle charge and rest mass, respectively. Under these conditions, the equilibrium self-electric and self-magnetic fields associated with an intense nonneutral charged-particle beam can be approximated by

$$\vec{E}^{(s)}(x,y,s) = -\left(\vec{e}_x\frac{\partial}{\partial x} + \vec{e}_y\frac{\partial}{\partial y}\right)\Phi^{(s)}(x,y,s) \ , \tag{5}$$

and

$$\vec{B}^{(s)}(x,y,s) = \left(\vec{e}_x\frac{\partial}{\partial y} - \vec{e}_y\frac{\partial}{\partial x}\right)A_z^{(s)}(x,y,s) \ , \tag{6}$$

where the scalar potential for the self-electric field obeys the Poisson equation

$$\left(\frac{\partial^2}{\partial x^2} + \frac{\partial^2}{\partial y^2}\right)\Phi^{(s)}(x,y,s) = -4\pi q n_0(x,y,s) \ , \tag{7}$$

and the vector potential for the self-magnetic field is given by

$$\vec{A}^{(s)}(x,y,s) = \beta_b\Phi^{(s)}(x,y,s)\vec{e}_z \ . \tag{8}$$

Throughout this paper, the equilibrium particle density $n_0(x,y,s)$ in Eq. (7) is assumed to be uniform over the cross section of the cylindrical beam with radius $r_b(s)$, i.e.,

$$n_0(x,y,s) = \begin{cases} N/\pi r_b^2(s) & \text{for } 0 \le r < r_b(s), \\ 0 & \text{for } r > r_b(s), \end{cases} \tag{9}$$

where $r = (x^2+y^2)^{1/2}$ is the radial coordinate, and $r_b(s) = r_b(s+S)$ is a periodic function of s. From Eqs. (7) and (9), the scalar potential within the beam is easily found to be

$$\Phi^{(s)}(x,y,s) = -\frac{qNr^2}{r_b^2(s)} \ . \tag{10}$$

The equations of motion in the laboratory frame can be derived from the single-particle Hamiltonian defined by

$$H(x,y,s,P_x,P_y,P_z)$$

$$= \left[c^2\left(P_x - \frac{q}{c}A_x^{(ext)}\right)^2 + c^2\left(P_y - \frac{q}{c}A_y^{(ext)}\right)^2 + c^2\left(P_z - \frac{q}{c}A_z^{(s)}\right)^2 + m^2c^4\right]^{1/2} + q\Phi^{(s)} \ , \tag{11}$$

where (s, P_z) is a canonical conjugate pair and the canonical momentum $\vec{P}$ is related to the mechanical momentum $\vec{p}$ by $\vec{P} = \vec{p} + (q/c)[\vec{A}^{(\mathrm{ext})} + \vec{A}^{(\mathrm{s})}]$. Here, $s = \beta_b ct$ is the axial coordinate, where $\beta_b c$ is the average axial velocity of the beam particles. Because the transverse motion is assumed to be nonrelativistic in the paraxial approximation, the axial mechanical momentum $p_z = \gamma_b m \beta_b c$ can be treated approximately as a constant. Hence, the full Hamiltonian can be approximated by

$$H = \gamma_b mc^2 + H_\perp \,, \tag{12}$$

where $\gamma_b = (1 - \beta_b^2)^{1/2} = \text{const.}$, and the Hamiltonian for the transverse motion is defined by

$$H_\perp(x, y, P_x, P_y, s) = \frac{1}{2\gamma_b m}\left[\left(P_x + \frac{qB_z(s)}{2c}y\right)^2 + \left(P_y - \frac{qB_z(s)}{2c}x\right)^2\right] - \frac{q^2 N}{\gamma_b r_b^2(s)}(x^2 + y^2) \,, \tag{13}$$

where $s = \beta_b ct$ is the axial coordinate.

It is useful to introduce the normalized transverse canonical momenta and Hamiltonian,

$$\hat{P}_x = \frac{P_x}{\gamma_b m \beta_b c}, \quad \hat{P}_y = \frac{P_y}{\gamma_b m \beta_b c}, \quad \hat{H}_\perp = \frac{H_\perp}{\gamma_b m \beta_b^2 c^2} \,, \tag{14}$$

the normalized focusing strength parameter,

$$\sqrt{\kappa_z(s)} = \frac{qB_z(s)}{2\gamma_b \beta_b mc^2} \,, \tag{15}$$

and the normalized self-field strength parameter,

$$\kappa_s(s) = \frac{K}{r_b^2(s)} \,, \tag{16}$$

where $K = 2\nu/\gamma_b^3\beta_b^2 = 2q^2N/\gamma_b^3\beta_b^2 mc^2$ is the normalized perveance of the beam. Making use of the above notations, the normalized Hamiltonian for the transverse motion can be expressed as

$$\hat{H}_\perp(x, y, \hat{P}_x, \hat{P}_y, s) = \frac{1}{2}\left\{\left[\hat{P}_x + y\sqrt{\kappa_z(s)}\right]^2 + \left[\hat{P}_y - x\sqrt{\kappa_z(s)}\right]^2 - \kappa_s(s)(x^2 + y^2)\right\} \,, \tag{17}$$

where the axial distance $s = \beta_b ct$ is an effective time variable. The equations of motion for a single particle in the laboratory frame are given by

$$x' = \frac{\partial \hat{H}_\perp}{\partial \hat{P}_x} = \hat{P}_x + y\sqrt{\kappa_z(s)} \ ,$$

$$y' = \frac{\partial \hat{H}_\perp}{\partial \hat{P}_y} = \hat{P}_y - x\sqrt{\kappa_z(s)} \ ,$$

$$\hat{P}_x' = -\frac{\partial \hat{H}_\perp}{\partial x} = \hat{P}_y\sqrt{\kappa_z(s)} - [\kappa_z(s) - \kappa_s(s)]x \ , \tag{18}$$

$$\hat{P}_y' = -\frac{\partial \hat{H}_\perp}{\partial y} = -\hat{P}_x\sqrt{\kappa_z(s)} - [\kappa_z(s) - \kappa_s(s)]y \ .$$

Note that the motion in the x-direction is strongly coupled to the motion in the y-direction in the laboratory frame.

B. Equations of Motion in the Larmor Frame

We now perform a canonical transformation from the laboratory frame to the so-called Larmor frame [2] which rotates with respect to the laboratory frame with angular velocity $\beta_b c\sqrt{\kappa_z(s)} = qB_z(s)/2\gamma_b mc$, i.e., at one-half of the *local* relativistic cyclotron frequency. The generating function for such a transformation from $(x, y, \hat{P}_x, \hat{P}_y)$ to $(\tilde{x}, \tilde{y}, \tilde{P}_x, \tilde{P}_y)$ can be chosen as

$$F_2(x, y; \tilde{P}_x, \tilde{P}_y, s) = \{x\cos[\phi(s)] - y\sin[\phi(s)]\}\tilde{P}_x + \{x\sin[\phi(s)] + y\cos[\phi(s)]\}\tilde{P}_y \ , \tag{19}$$

where $\phi(s) = \int_{s_0}^{s} ds\sqrt{\kappa_z(s)}$. The generating function F_2 defines the following transformation

$$\tilde{x} = x\cos[\phi(s)] - y\sin[\phi(s)] \ ,$$

$$\tilde{y} = x\sin[\phi(s)] + y\cos[\phi(s)] \ ,$$

$$\tilde{P}_x = \hat{P}_x\cos[\phi(s)] - \hat{P}_y\sin[\phi(s)] \ , \tag{20}$$

$$\tilde{P}_y = \hat{P}_x\sin[\phi(s)] + \hat{P}_y\cos[\phi(s)] \ .$$

The Hamiltonian in the new variables $(\tilde{x}, \tilde{y}, \tilde{P}_x, \tilde{P}_y)$ can then be expressed as

$$\tilde{H}_\perp(\tilde{x}, \tilde{y}, \tilde{P}_x, \tilde{P}_y, s) = \frac{1}{2}[\tilde{P}_x^2 + \tilde{P}_y^2 + \kappa(s)(\tilde{x}^2 + \tilde{y}^2)] \ , \tag{21}$$

where $\kappa(s) = \kappa_x(s) - \kappa_s(s)$, and use has been made of the property that $\tilde{H}_\perp = \hat{H}_\perp + \partial F_2/\partial s$. The equations of motion in the Larmor frame are given by

$$\tilde{x}' = \tilde{P}_x \ , \tag{22}$$

$$\tilde{y}' = \tilde{P}_y \ , \tag{23}$$

$$\tilde{P}_x' = -\kappa(s)\tilde{x} \ , \tag{24}$$

$$\tilde{P}_y' = -\kappa(s)\tilde{y} \ . \tag{25}$$

Combining Eqs. (22) and (24) gives

$$\frac{d^2\tilde{x}}{ds^2} + \kappa(s)\tilde{x} = 0 \ . \tag{26}$$

Similarly, from Eqs. (23) and (25), we obtain

$$\frac{d^2\tilde{y}}{ds^2} + \kappa(s)\tilde{y} = 0 \ . \tag{27}$$

For an even periodic function $\kappa(s) = \kappa(-s) = \kappa(s + S)$, which is a special case of the present analysis, Eq. (26) or Eq. (27) is known as Hill's equation.

Two remarks are in order regarding the canonical transformation in Eq. (20) from the laboratory frame to the Larmor frame. First, because the transformation is a pure rotation, it preserves the invariance of an arbitrary axisymmetric equilibrium density profile, i.e., $n_0(r, s) = n_0(\tilde{r}, s)$, where $\tilde{r} = (\tilde{x}^2 + \tilde{y}^2)^{1/2}$. Second, the motion in the $\tilde{x}$-direction is decoupled from the motion in the $\tilde{y}$-direction for the uniform density profile defined in Eq. (9). Such decoupling can be accomplished with a pure rotation if and only if the equilibrium density profile is both axisymmetric and uniform within the beam.

III. KAPCHINSKIJ-VLADIMIRSKIJ DISTRIBUTION FUNCTION

The Kapchinskij-Vladimirskij (K-V) distribution [4] is the only known self-consistent Vlasov equilibrium ($\partial/\partial s = 0$) for an intense charged-particle beam in a periodic linear focusing field including self-field effects. Such a periodic focusing field can be realized either in an alternating-gradient quadrupole magnetic field configuration in the laboratory frame or in a periodic solenoidal magnetic field configuration in the Larmor frame as shown in Sec. II. Because the latter configuration possesses a higher degree of symmetry than the former, there are subtle differences between the two configurations. The aim of this section is to construct the K-V distribution function for a periodic solenoidal magnetic field configuration and to point out the differences between the periodic solenoidal and alternating-gradient quadrupole magnetic field configurations.

To construct the K-V equilibrium distribution function for an intense charged-particle beam propagating through a periodic solenoidal magnetic field, we adapt Courant and Snyder's treatment [18] of the alternating-gradient synchrotron, noting the symmetry that $\kappa_x(s) = \kappa_y(s) = \kappa(s)$. We define

$$\tilde{x}(s) = A_x w(s) \cos\left[\int_{s_0}^{s} \frac{ds}{w^2(s)} + \Psi_{x0}\right] \tag{28}$$

and

$$\tilde{y}(s) = A_y w(s) \sin\left[\int_{s_0}^{s} \frac{ds}{w^2(s)} + \Psi_{y0}\right] . \tag{29}$$

In Eqs. (28) and (29), $w(s) = w(s + S)$ is the square-root of the so-called amplitude function, and A_x, A_y, Ψ_{x0} and Ψ_{y0} are constants which can be determined from the "initial" conditions $\tilde{x}(s_0)$, $\tilde{y}(s_0)$, $\tilde{P}_x(s_0) = \tilde{x}'(s_0)$, and $\tilde{P}_y(s_0) = \tilde{y}'(s_0)$. Substituting Eq. (28) into Eqs. (22) and (24), and Eq. (29) into Eqs. (23) and (25), we find that Eqs. (28) and (29) solve the Hamilton equations (22)-(25), provided $w(s)$ solves the differential equation [18]

$$\frac{d^2w}{ds^2} + \kappa(s)w = \frac{1}{w^3} \tag{30}$$

subject to the periodicity constraint $w(s) = w(s+S)$.

It is convenient to make the canonical transformation from $(\tilde{x}, \tilde{y}, \tilde{P}_x, \tilde{P}_y)$ to the new variables (X, Y, P_X, P_Y) defined by [10]

$$\begin{aligned} X &= \frac{\tilde{x}}{w} , \\ Y &= \frac{\tilde{y}}{w} , \\ P_X &= w\tilde{P}_x + \frac{dw}{ds}\tilde{x} , \\ P_Y &= w\tilde{P}_y + \frac{dw}{ds}\tilde{y} , \end{aligned} \tag{31}$$

with the generating function

$$\tilde{F}_2(\tilde{x}, \tilde{y}; P_X, P_Y, s) = \frac{\tilde{x}}{w}\left(P_X + \frac{\tilde{x}}{2}\frac{dw}{ds}\right) + \frac{\tilde{y}}{w}\left(P_Y + \frac{\tilde{y}}{2}\frac{dw}{ds}\right) . \tag{32}$$

The Hamiltonian in the new variables (X, Y, P_X, P_Y) can be expressed as

$$H(X, Y, P_X, P_Y, s) = \frac{1}{2w^2(s)}(X^2 + Y^2 + P_X^2 + P_Y^2) , \tag{33}$$

which is proportional to the sum of the following two independent constants of the motion,

$$A_x^2 = X^2 + P_X^2 = \text{const.} , \tag{34}$$

and

$$A_y^2 = Y^2 + P_Y^2 = \text{const.} \tag{35}$$

The constancy of the quantities $X^2 + P_X^2$ and $Y^2 + P_Y^2$ is readily verified from Eqs. (28), (29) and (31).

The Kapchinskij-Vladimirskij distribution function [4] can be expressed as

$$f_0(X, Y, P_X, P_Y) = \frac{N}{\pi^2\epsilon}\delta(X^2 + Y^2 + P_X^2 + P_Y^2 - \epsilon) , \tag{36}$$

which describes a class of self-consistent Vlasov equilibria ($\partial/\partial s = 0$) for an intense charged-particle beam in a periodic solenoidal magnetic field including the effects of the

self-electric and self-magnetic fields [1] associated with the beam space-charge and current. In Eq. (36), the parameter ϵ is the unnormalized emittance of the beam. Integrating f_0 over the momentum space (P_X, P_Y), we find that the particle density $n_0(x, y, s)$ is given by the step-function profile in Eq. (9) provided

$$r_b(s) = \epsilon^{1/2} w(s) \ . \tag{37}$$

Therefore, the assumption made regarding the density profile in Sec. II is consistent with the choice of the K-V distribution function in Eq. (36).

The relationship in Eq. (37) can be derived independently by observing the axisymmetry of the beam and the fact that the beam radius $r_b(s)$ corresponds to the maximum value achieved by $\tilde{x}(s)$ along the $\tilde{x}$-axis when $A_y = 0$. Indeed, setting $A_x = A_x^{\max} = \sqrt{\epsilon}$ and $\cos[\Psi_{x0} + \int_{s_0}^{s} ds/w^2(s)] = 1$ in Eq. (28) yields Eq. (37). From Eqs. (30) and (37), we obtain the beam envelope equation

$$\frac{d^2 r_b}{ds^2} + \kappa_z(s) r_b - \frac{K}{r_b} - \frac{\epsilon^2}{r_b^3} = 0 \ , \tag{38}$$

where use has been made of the relation $\kappa(s) = \kappa_z(s) - \kappa_s(s)$ and Eq. (16). Equation (38) is also referred to as the Kapchinskij-Vladimirskij equation in the literature.

In the present solenoidal magnetic field configuration, the beam envelope evolution is described by a *single* second-order ordinary differential equation because of the axisymmetry in both the applied focusing field and the beam density profile. This is in contrast to the case of alternating-gradient quadrupole magnetic field configuration [4] in which the K-V equilibrium corresponds to a beam whose density is uniform over an elliptical area of the beam cross section and whose envelope must be described by two coupled second-order ordinary differential equations [1, 4].

To complete the construction of the K-V distribution function for an intense charged-particle beam in a periodic solenoidal focusing field, periodic solutions to Eq. (38) remain to be found. The procedure for finding a stable periodic solution to Eq. (38) with

periodicity length S is often referred to as *beam matching*, which will be discussed in Sec. IV. For a matched (equilibrium) beam, the phase advance over an axial period of the focusing field is defined by

$$\sigma \equiv \int_{s_0}^{s_0+S} \frac{ds}{w^2(s)} = \epsilon \int_{s_0}^{s_0+S} \frac{ds}{r_b^2(s)} , \tag{39}$$

where use has been made of Eq. (37). As shown in Sec. IV, the phase advance without space-charge, i.e., $\sigma_0 = \sigma|_{K=0}$, is an important parameter characterizing the focusing field.

The unnormalized emittance ϵ in Eq. (36) is a measure of the phase-space area occupied by the beam. Indeed, it is readily shown [18] from Eq. (38) that $\pi\epsilon$ is equal to the minimum area, in either the phase plane (X, P_X) or the phase plane (Y, P_Y), required to enclose all of the particles described by the K-V distribution function f_0. Furthermore, it is straightforward to show that the unnormalized emittance ϵ is equal to the rms emittance defined by [5, 6]

$$\epsilon_{\rm rms} = 4[\langle X^2\rangle\langle P_X^2\rangle - \langle XP_X\rangle^2]^{1/2} . \tag{40}$$

In Eq. (40), the average of the phase function $\chi(X, Y, P_X, P_Y)$ over the phase space (X, Y, P_X, P_Y) is defined by

$$\langle\chi\rangle = \frac{\int \chi f_0 d\Gamma}{\int f_0 d\Gamma} , \tag{41}$$

where $d\Gamma = dXdYdP_XdP_Y$.

Finally, we derive an important equation which relates the unnormalized emittance ϵ and the maximum canonical angular momentum $P_{\theta m}$ allowed for the particles within the K-V distribution. Making use of Eqs. (14), (20), (28) and (29), we can express the canonical angular momentum for an individual particle within the K-V distribution as

$$P_\theta = xP_y - yP_x = A_xA_y(\gamma_b m\beta_b c)\cos(\Psi_{x0} - \Psi_{y0}) = \text{const.} , \tag{42}$$

where the amplitudes A_x and A_y satisfy the relation $A_x^2 + A_y^2 = \epsilon$, and Ψ_{x0} and Ψ_{y0} are the "initial" phases for the particle motion in the $\tilde{x}$- and $\tilde{y}$-directions, respectively. It is

readily shown that P_θ obeys the inequality

$$-P_{\theta m} \leq P_\theta \leq P_{\theta m} \ , \tag{43}$$

where the maximum canonical angular momentum is given by

$$P_{\theta m} = \frac{1}{2}\epsilon\gamma_b m\beta_b c \ . \tag{44}$$

It can also be shown that the particles with $P_\theta = \pm P_{\theta m}$ always stay at the rms beam radius [i.e., at $r(s) = r_b(s)/\sqrt{2}$], whereas the particles instantaneously reaching the beam edge $r(s) = r_b(s)$ carry *zero* canonical angular momentum.

IV. BEAM MATCHING INTO THE FOCUSING FIELD

The aim of this section is to study the properties of the beam envelope equation (38) and present a numerical method for finding periodic solutions to Eq. (38). For present purposes, we introduce the *dimensionless* parameters and variables defined by

$$\frac{s}{S} \to s \ , \quad \frac{r_b}{\sqrt{\epsilon S}} \to r_b \ , \quad S^2\kappa_z \to \kappa_z \ , \quad \frac{SK}{\epsilon} \to K \ , \tag{45}$$

and express Eq. (38) in the following normalized form

$$\frac{d^2 r_b}{ds^2} + \kappa_z(s) r_b - \frac{K}{r_b} - \frac{1}{r_b^3} = 0 \ . \tag{46}$$

Equation (46) is equivalent to the first-order ordinary differential equations

$$\frac{dr_b}{ds} = r_b' \tag{47}$$

and

$$\frac{dr_b'}{ds} = -\kappa_z(s) r_b + \frac{K}{r_b} + \frac{1}{r_b^3} \ . \tag{48}$$

The normalized beam envelope equation (46) is now characterized by two parameters, namely, $\kappa_z(s)$ and K, which measure the (focusing) strength of the applied periodic solenoidal magnetic field and the (defocusing) strength of the equilibrium self fields of the beam, respectively. Unless specified otherwise, the dimensionless parameters and variables defined in Eq. (45) will be used in the remainder of the paper.

By making a Fourier expansion of the axial magnetic field profile $B_z(s) = B_z(s+1)$, we express the normalized focusing strength parameter $\kappa_z(s)$ as

$$\kappa_z(s) = \left\{ \sum_{n=0}^{\infty} [a_n \cos(2n\pi s) + b_n \sin(2n\pi s)] \right\}^2 \ , \tag{49}$$

where the coefficients a_n and b_n are proportional to the coefficients in the Fourier expansion for $B_z(s)$. Moreover, $\kappa_z(s)$ can be decomposed according to

$$\kappa_z(s) = \kappa_z^{(+)}(s) + \kappa_z^{(-)}(s) \ , \tag{50}$$

where the periodic functions $\kappa_z^{(\pm)}(s) = \kappa_z^{(\pm)}(s+1) = \pm\kappa_z^{(\pm)}(-s)$ are defined by

$$\kappa_z^{(+)}(s) = \frac{1}{2}[\kappa_z(s) + \kappa_z(-s)] = a_0^2 + \sum_{n=1}^{\infty}[a_n^2 \cos^2(2n\pi s) + b_n^2 \sin^2(2n\pi s)] \qquad (51)$$

and

$$\kappa_z^{(-)}(s) = \frac{1}{2}[\kappa_z(s) - \kappa_z(-s)] = 2\sum_{n=0}^{\infty}\sum_{m=1}^{\infty} a_n b_m \cos(2n\pi s)\sin(2m\pi s)\ . \qquad (52)$$

We refer to a focusing field with $\kappa_z(s) = \kappa_z^{(+)}(s)$ as an *even* focusing field. A sufficient condition for $\kappa_z(s) = \kappa_z^{(+)}(s)$ is that $b_n = 0$.

A. Poincaré Map Deduced from the Beam Envelope Equation

Periodic solutions to Eq. (46) with unit periodicity can be found using the *Poincaré mapping technique* [17] which tracks an ensemble of phase-space trajectories as they intersect the phase plane (r_b, r_b') located at successive axial positions $s = 0, 1, 2, \cdots$. Formally, we may express such a map as

$$\begin{pmatrix} r_b \\ r_b' \end{pmatrix}_{n+1} = \mathsf{T}\begin{pmatrix} r_b \\ r_b' \end{pmatrix}_n = \begin{pmatrix} \zeta(r_b, r_b') \\ \xi(r_b, r_b') \end{pmatrix}_n , \quad n = 0, \pm 1, \pm 2, \cdots, \qquad (53)$$

which maps the phase plane (r_b, r_b') onto itself from $s = n$ to $n+1$. Because Eq. (46) is a Hamiltonian system, it follows that the map preserves area in the phase plane. In the present analysis, the functions $\zeta(r_b, r_b')$ and $\xi(r_b, r_b')$ are obtained implicitly by integrating Eqs. (47) and (48) numerically with the fourth-order Runge-Kutta algorithm. In general, they have a highly nonlinear dependence on their arguments.

A periodic solution to Eq. (46), or equivalently to Eqs. (47) and (48), corresponds to a *fixed point* of the map defined by

$$\begin{pmatrix} \bar{r}_b \\ \bar{r}_b' \end{pmatrix} = \mathsf{T}\begin{pmatrix} \bar{r}_b \\ \bar{r}_b' \end{pmatrix} . \qquad (54)$$

In principle, such a fixed point may correspond to a periodic solution with a fundamental periodicity of $1/m$, where $m = 1, 2, \cdots$. Linearizing T about the fixed point yields the

tangent map defined by

$$\begin{pmatrix} \delta r_b \\ \delta r_b' \end{pmatrix} = \begin{pmatrix} \frac{\partial \zeta}{\partial r_b} & \frac{\partial \zeta}{\partial r_b'} \\ \frac{\partial \xi}{\partial r_b} & \frac{\partial \xi}{\partial r_b'} \end{pmatrix}_{(\bar{r}_b, \bar{r}_b')} \begin{pmatrix} \delta r_b \\ \delta r_b' \end{pmatrix} , \tag{55}$$

where $\delta r_b = r_b - \bar{r}_b$ and $\delta r_b' = r_b' - \bar{r}_b'$ are small quantities. A fixed point is *stable* if the eigenvalues of the tangent map about that fixed point are of unit module. It should be emphasized that as far as completing the construction of the K-V distribution function in Sec. III is concerned, we are interested in locating the stable fixed points of the map.

In the limit of a uniform solenoidal magnetic field with $\kappa_z(s) = \kappa_{z0} = \text{const.}$, it is readily shown that the beam envelope equation (46) is *integrable* and possesses a unique stable steady-state solution given by [1]

$$r_b(s) = r_{b0} = \left\{ \left[\left(\frac{K}{2\kappa_{z0}} \right)^2 + \frac{1}{\kappa_{z0}} \right]^{1/2} + \frac{K}{2\kappa_{z0}} \right\}^{1/2} . \tag{56}$$

Therefore, the point $(\bar{r}_b, \bar{r}_b') = (r_{b0}, 0)$ is a unique stable fixed point of T. As K is increased, the beam radius expands due to the (defocusing) self-field effects. Indeed, the *Brillouin flow condition* [1, 19], i.e., $r_{b0}^2 = K/\kappa_{z0}$, is recovered as $\epsilon \to 0$, or equivalently the normalized perveance parameter $K \to \infty$ [see Eq. (45)]. Since both of the normalized quantities K and r_{b0}^2 are inversely proportional to ϵ, as defined in Eq. (45), the Brillouin flow condition can be expressed in the familiar dimensional form [1]

$$\frac{2\omega_{pb}^2}{\gamma_b \omega_c^2} = 1 , \tag{57}$$

where $\omega_{pb} = (4q^2 N/m r_{b0}^2)^{1/2}$ is the nonrelativistic plasma frequency of the beam particles and $\omega_c = qB_z/mc$ is the nonrelativistic cyclotron frequency.

For general focusing field, however, the beam envelope equation (46) describes a Hamiltonian system with one and one-half degrees of freedom, and therefore is generally *nonintegrable*. The Poincaré map T is expected to generate a mixture of *regular* and *chaotic* orbits in the phase plane (r_b, r_b'). In practice, the fixed-point equation (54) must be solved numerically.

Unlike the beam envelope equation (38), the differential equation (30) for the amplitude function $w(s)$ (in the dimensional form),

$$\frac{d^2w}{ds^2} + \left[\kappa_z(s) - \frac{K}{r_b^2(s)}\right]w = \frac{1}{w^3} , \tag{58}$$

is integrable in the parameter regime where the radius of the matched (equilibrium) beam is given by a periodic solution to Eq. (38). This is because the underlying equations (26) and (27) for this case are *linear* ordinary differential equations, where $\kappa(s) = \kappa(s+S) = \kappa_z(s) - K/r_b^2(s)$ is a *prescribed* periodic function.

The Poincaré map T has the important property that for an *even* focusing field with $\kappa_z(s) = \kappa_z(-s)$, the line $r_b' = 0$ (r_b-axis) is an axis of symmetry of the map T; that is, the phase plane (r_b, r_b') is symmetric with respect to the r_b-axis. This symmetry follows from the fact that Eqs. (47) and (48) are invariant under the transformation $(s, r_b, r_b') \rightarrow (-s, r_b, -r_b')$. Furthermore, it can be shown that for a focusing field with small-amplitude oscillations about $\kappa_z(s) = \kappa_{z0} = \text{const.}$, the fixed point of the map corresponds to the intersection of the r_b-axis and its image, as shown in Fig. 1. This fixed point originates from the value of r_{b0} defined in Eq. (56).

B. Beam Matching into an Even Focusing Field

With regard to the construction of the K-V distribution function, we must answer the questions of whether the map T has a unique fixed point, and if so, under what condition is the fixed point stable. To find definitive answers to these important questions, we consider a focusing field described by the even function

$$\kappa_z(s) = [a_0 + a_1 \cos(2\pi s)]^2 , \tag{59}$$

which physically also corresponds to a rather general class of even periodic axial magnetic field $B_z(s)$, truncated to leading order in the Fourier expansion. Figure 2 shows the phase plane (r_b, r_b') produced by successive applications of the Poincaré map with 20 initial

points on the r_b-axis. The choice of system parameters in Fig. 2 corresponds to: $K = 10$ and $a_0 = 1.07$ for the cases (a) $a_1 = 0$, (b) $a_1 = 1.07$, and (c) $a_1 = 2.85$.

In Fig. 2(a), the phase plane is completely regular (integrable), as expected for a uniform solenoidal magnetic field. The stable fixed point is located at $r_b = r_{b0} = 3.0$ on the r_b-axis, which is in agreement with Eq. (56). The elliptical orbits surrounding the fixed point represent stable (nonequilibrium) beam envelope oscillations about the matched (equilibrium) beam envelope $r_b(s) = r_{b0}$.

As the parameter a_1 is increased from $a_1 = 0$ to $a_1 = 1.07$, the stable fixed point moves slightly towards the origin, as shown in Fig. 2(b). The location of the fixed point corresponds to the intersection of the r_b-axis and its image shown in Fig. 1. In the vicinity of the fixed point, a pair of stable and unstable period-three orbits appear. Because the phase advance without space-charge is $\sigma_0 = \sigma|_{K=0} = 75°$, the appearance of the period-three resonance is well correlated with the third-order instability [10] for the K-V equilibrium, which occurs over a wide range of K when $\sigma_0 > 60°$.

While the area occupied by the chaotic orbits is hardly visible in Fig. 2(b), transition to a high degree of chaos in the phase plane is inevitable as a_1 is increased. Such a transition is accompanied by the shrinkage of the regular region surrounding the stable fixed point. This is illustrated in Fig. 2(c), where the stable fixed point is located at $r_b \cong 1.7$ on the r_b-axis. This fixed point is completely enveloped by chaotic orbits as a_1 is further increased.

In addition to apparent correlations between the nonlinear resonances in nonequilibrium beam envelope oscillations and the well-known instabilities [10] for the K-V equilibrium, the nonlinear resonances and chaotic behavior are expected to play an important role in the transport of mismatched or multiple beams, where large-amplitude, nonequilibrium beam envelope oscillations occur and can become chaotic. An intriguing phenomenon in mismatched or multiple beam transport is the formation and growth of

a beam halo.

For the cases shown in Fig. 2, the fact that the Poincaré map T possesses a unique stable fixed point demonstrates that the beam envelope equation (46) has a unique stable periodic solution with unit periodicity, and therefore there exists a unique K-V equilibrium distribution function. As a byproduct of determining the stable fixed point of the map, the stable periodic solution is obtained and shown in Fig. 3 for the case corresponding to Fig. 2(b). The phase advance defined in Eq. (39) is evaluated to be $\sigma = 10°$ with space-charge, and $\sigma_0 = \sigma|_{K=0} = 75°$ without space-charge.

Is it true that the map T can have at most *one* fixed point as suggested from the results shown in Fig. 2? A positive answer to this question is found by searching numerically all of the fixed points of the map over an extensive domain in the parameter space (K, a_0, a_1). As $|a_1|$ is increased, however, such a unique fixed point either destabilizes for $a_0 = 0$ or disappears for $a_0 \neq 0$. Figure 4 shows the boundary in the parameter plane $(K, |a_1|)$ below which the map T has a unique stable fixed point.

It should be pointed out that the threshold for the destabilization or disappearance of the fixed point, as measured by the phase advance without space-charge σ_0, is found to be greater than the threshold for the birth of a pair of stable and unstable period-two orbits which occurs at $\sigma_0 \approx 90°$. Because the phase advance without space charge σ_0 is

$$\sigma_0^2 = \int_0^1 \kappa_z(s)ds = a_0^2 + \frac{a_1^2}{2} \tag{60}$$

in the smooth-beam approximation, the threshold for the birth of the period-two orbits is given approximately by

$$a_0^2 + \frac{a_1^2}{2} = \frac{\pi^2}{4} \,. \tag{61}$$

The numerical results shown in Fig. 5 confirm this condition.

Finally, we note for $\sigma_0 > 90°$, that the Kapchinskij-Vladimirskij equilibrium distribution function is subject to the strong, second-order (envelope) instability [10] over a wide range of K. Therefore, we conclude that in the parameter regime of practical interest

[i.e., $\sigma_0 < 90°$ or $a_0^2 + (1/2)a_1^2 < \pi^2/4$], there exists a uniquely matched beam whose radius is given by the stable periodic solution $r_b(s) = r_b(s+1)$ to the beam envelope equation (46).

V. CONCLUSIONS

The basic properties of the Kapchinskij-Vladimirskij (K-V) equilibrium and beam envelope equation have been explored for intense charged-particle beam propagation through a periodic solenoidal focusing magnetic field including the effects of the self-electric and self-magnetic fields associated with the beam space-charge and current. It was found that the unnormalized beam emittance is proportional to the maximum canonical angular momentum achieved by the particles in the K-V distribution. The Poincaré mapping technique was used in the analysis of the dynamics described by the beam envelope equation. This technique allowed us to determine systematically the axial dependence of the radius of the matched (equilibrium) beam and to explore nonlinear resonances in the nonequilibrium beam envelope oscillations. Certain correlations were found between the nonlinear resonances and well-known instabilities for the K-V equilibrium. It was shown, for the first time, that nonequilibrium beam envelope oscillations exhibit chaotic behavior for a periodic focusing magnetic field and sufficiently high beam density, and that there exists a uniquely matched beam in the parameter regime of practical interest, i.e., $\sigma_0 < 90°$, where σ_0 is the vacuum phase advance over an axial period of the focusing field neglecting beam self-field effects. Finally, effects of the nonlinear resonances and chaotic beam envelope oscillations on mismatched or multiple beam transport and the formation and evolution of beam halo are being studied by means of numerical simulation, and will be the subject of a future report. The present analysis can extended to the case of an alternating-gradient quadrupole magnetic field configuration.

ACKNOWLEDGMENTS

This work was supported in part by the Office of Naval Research and in part by the Department of Energy High Energy Physics Division.

References

[1] R.C. Davidson, *Physics of Nonneutral Plasmas* (Addison-Wesley, Reading, MA, 1990).

[2] J.D. Lawson, *Physics of Charged Particle Beams*, 2nd ed. (Oxford University Press, 1988).

[3] *Heavy Ion Inertial Fusion*, eds., M. Reiser, T. Godlove, and R. Bangerter, AIP Conf. Proc. No. 152, (AIP, New York, 1986), and references therein.

[4] I.M. Kapchinskij and V.V. Vladimirskij, Proc. Int. Conf. on High Energy Accelerators, CERN, Geneva (1959), p. 274.

[5] P.M. Lapostolle, IEEE Trans. Nucl. Sci. **NS-18**, 1101 (1971).

[6] F.J. Sacherer, IEEE Trans. Nucl. Sci. **NS-18**, 1105 (1971).

[7] J.D. Lawson, P.M. Lapostolle, and R.L. Gluckstern, Part. Accel. **5**, 61 (1973).

[8] E.P. Lee and R.K. Copper, Part. Accel. **7**, 83 (1976).

[9] M. Reiser, Part. Accel. **8**, 167 (1978).

[10] I. Hofmann, L.J. Laslett, L. Smith, and I. Haber, Part. Accel. **13**, 145 (1983).

[11] J. Struckmeier, J. Klabunde, and M. Reiser, Part. Accel. **15**, 47 (1984).

[12] T.P. Wangler, K.R. Crandall, R.S. Mills, and M. Reiser, IEEE Trans. Nucl. Sci. **NS-32**, 2196 (1985).

[13] O.A. Anderson, Part. Accel. **21**, 197 (1987).

[14] M. Reiser, C.R. Chang, D. Kelne, K. Low, T. Shea, H. Rudd, and I. Haber, Phys. Rev. Lett. **61**, 2933 (1988); I. Haber, D. Kelne, M. Reiser, and H. Rudd, Phys. Rev. **A44**, 5194 (1991).

[15] C.L. Bohn, Phys. Rev. Lett. **70**, 932 (1993).

[16] R.A. Jameson, private communication (1993).

[17] A.J. Lichtenberg and M.A. Lieberman, *Regular and Chaotic Motion*, 2nd ed. (Springer-Verlag, New York, 1992).

[18] E.D. Courant and H.S. Snyder, Annals of Physics **3**, 1 (1958).

[19] L. Brillouin, Phys. Rev. **67**, 260 (1945).

FIGURE CAPTIONS

Fig. 1. Plot of the r_b-axis (straight line) and its image (dashed curve) showing a unique intersection for the choice of the system parameters $K = 10$, and $\kappa(s) = (1.07)^2 \times [1 + \cos(2\pi s)]^2$.

Fig. 2. Poincaré surface-of-section plots showing the transition from regular orbits to chaotic orbits in the phase plane (r_b, r_b'). The choice of system parameters corresponds to: $K = 10$ and $a_0 = 1.07$ for the cases (a) $a_1 = 0$, (b) $a_1 = 1.07$, and (c) $a_1 = 2.85$. In each plot, 20 points, initially on the r_b-axis, are iterated 250 times (i.e., 250 axial periods of the focusing field).

Fig. 3. Plot of the beam radius $r_b(s)$ versus axial coordinate s for the case of a matched (equilibrium) beam and system parameters corresponding to Figs. 1 and 2(b).

Fig. 4. The threshold value of $|a_1|$ below which the map T has a unique stable fixed point is plotted as a function of normalized perveance K. The solid line connecting the open circles is obtained for $a_0 = 0$, and the solid line connecting the open squares is obtained for $a_0 = 1.07$.

Fig. 5. The threshold curve for the birth a pair of stable and unstable period-two orbits is plotted in the parameter space (a_0, a_1) for K = 10. The open circles are numerical results, whereas the solid curve is given by Eq. (61).

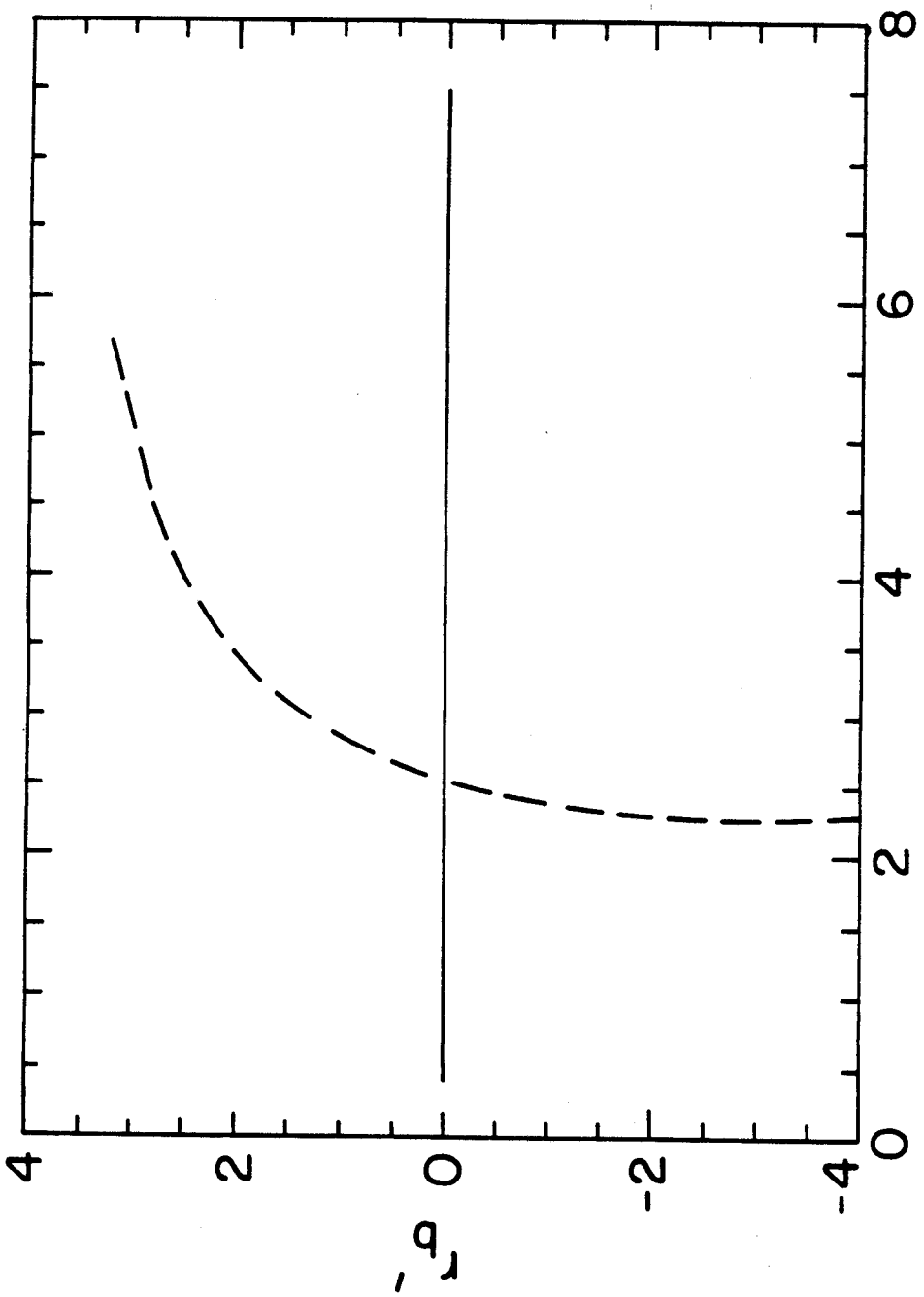

Figure 1

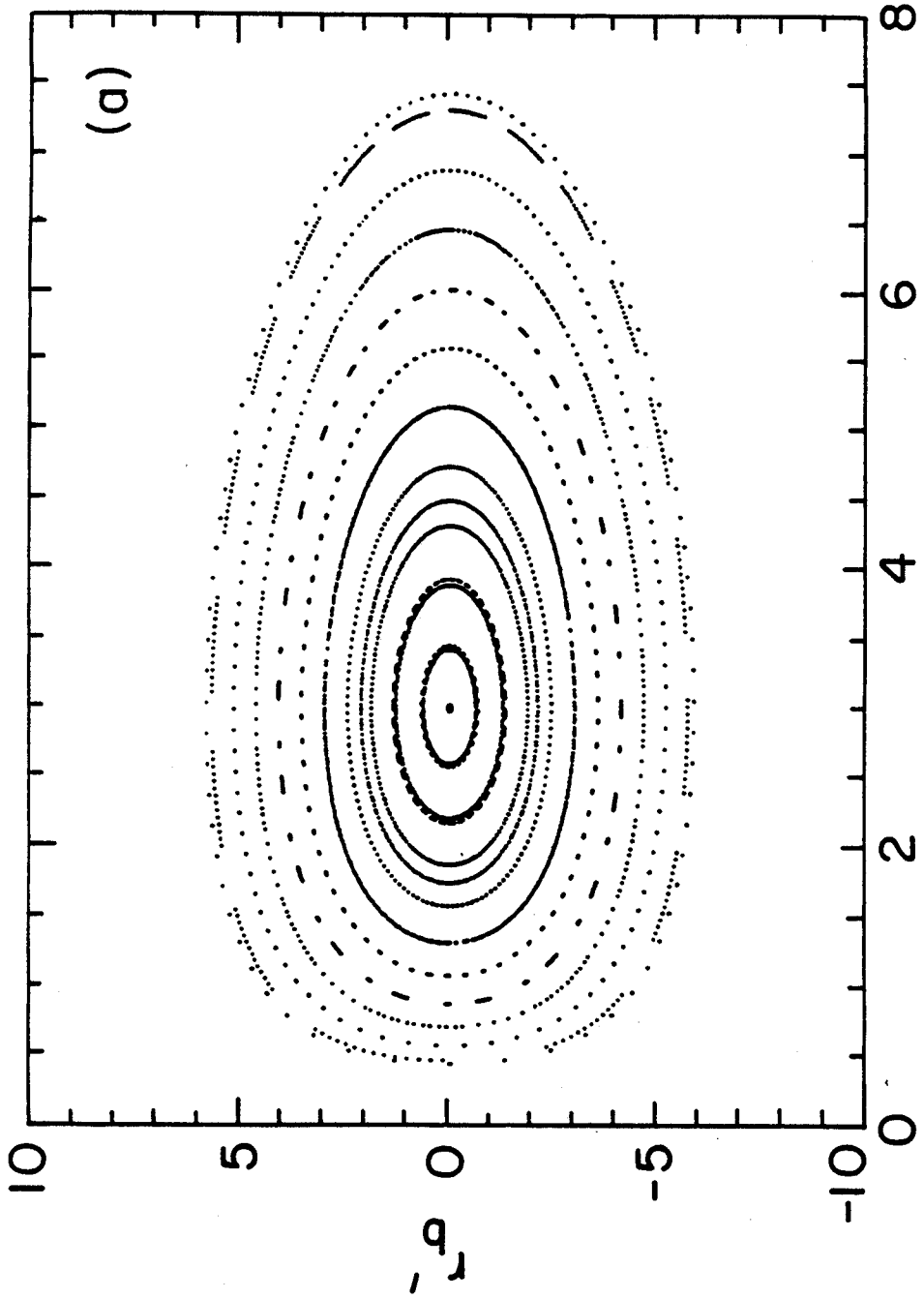

Figure 2(a)

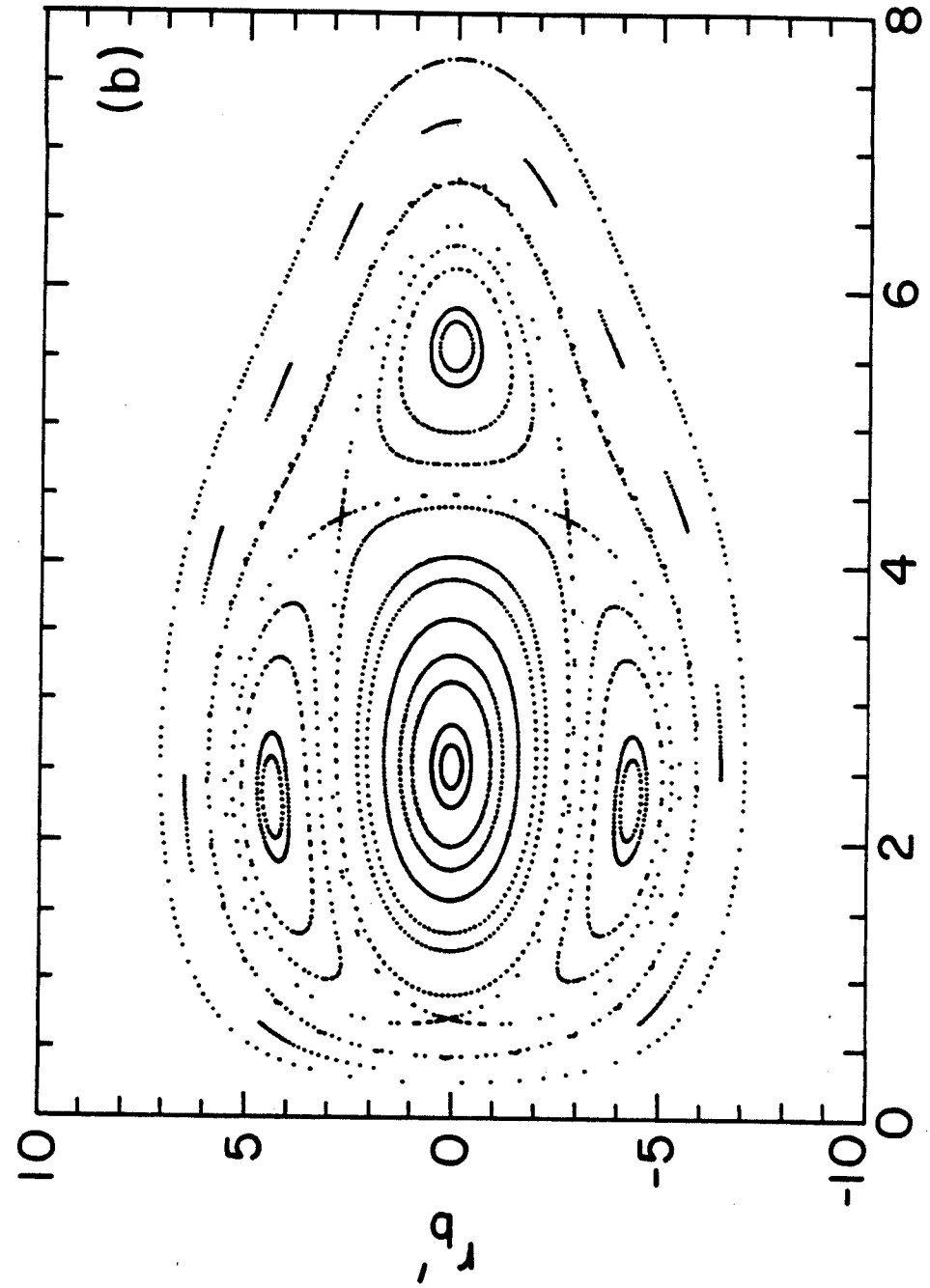

Figure 2(b)

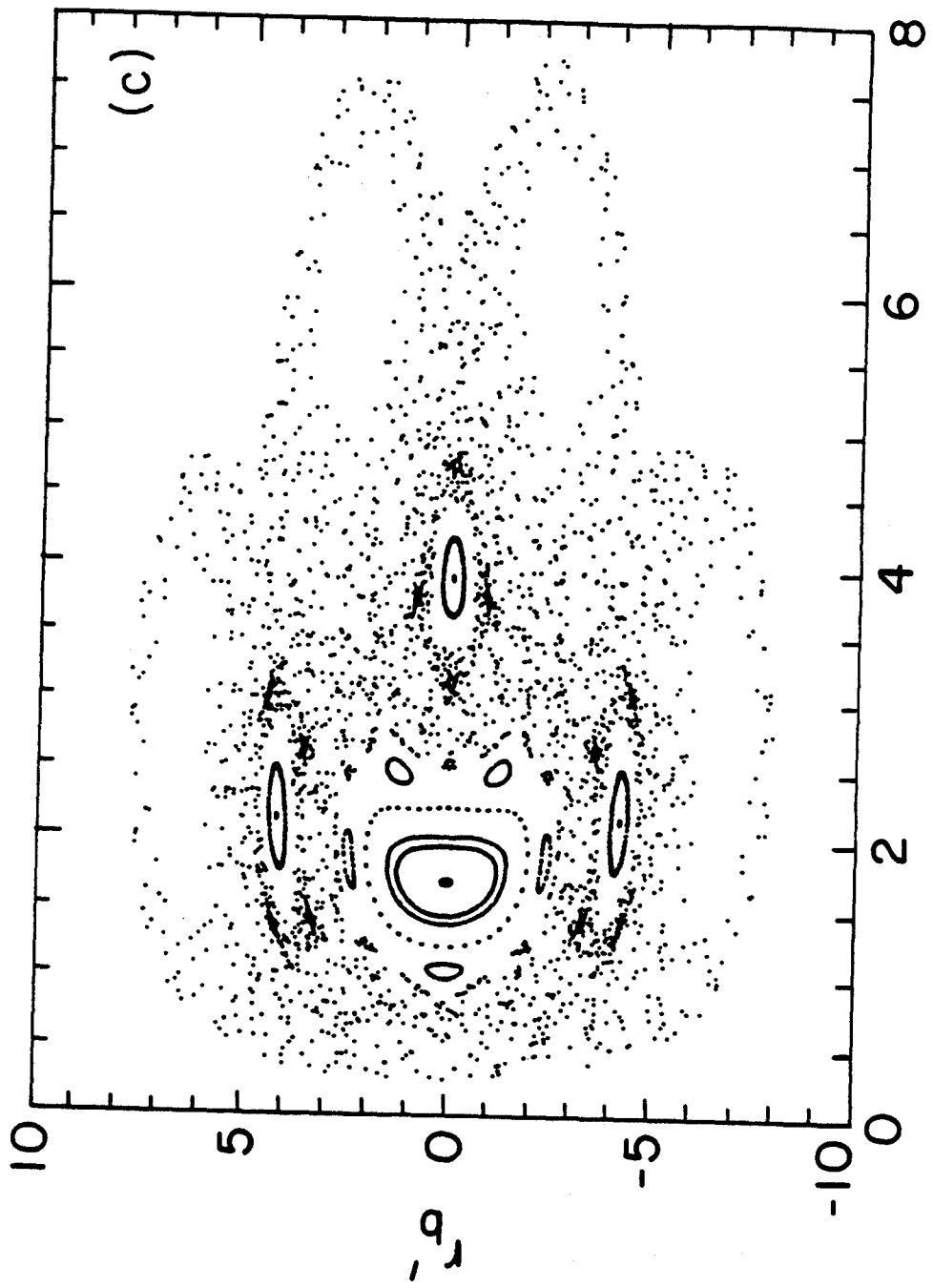

Figure 2(c)

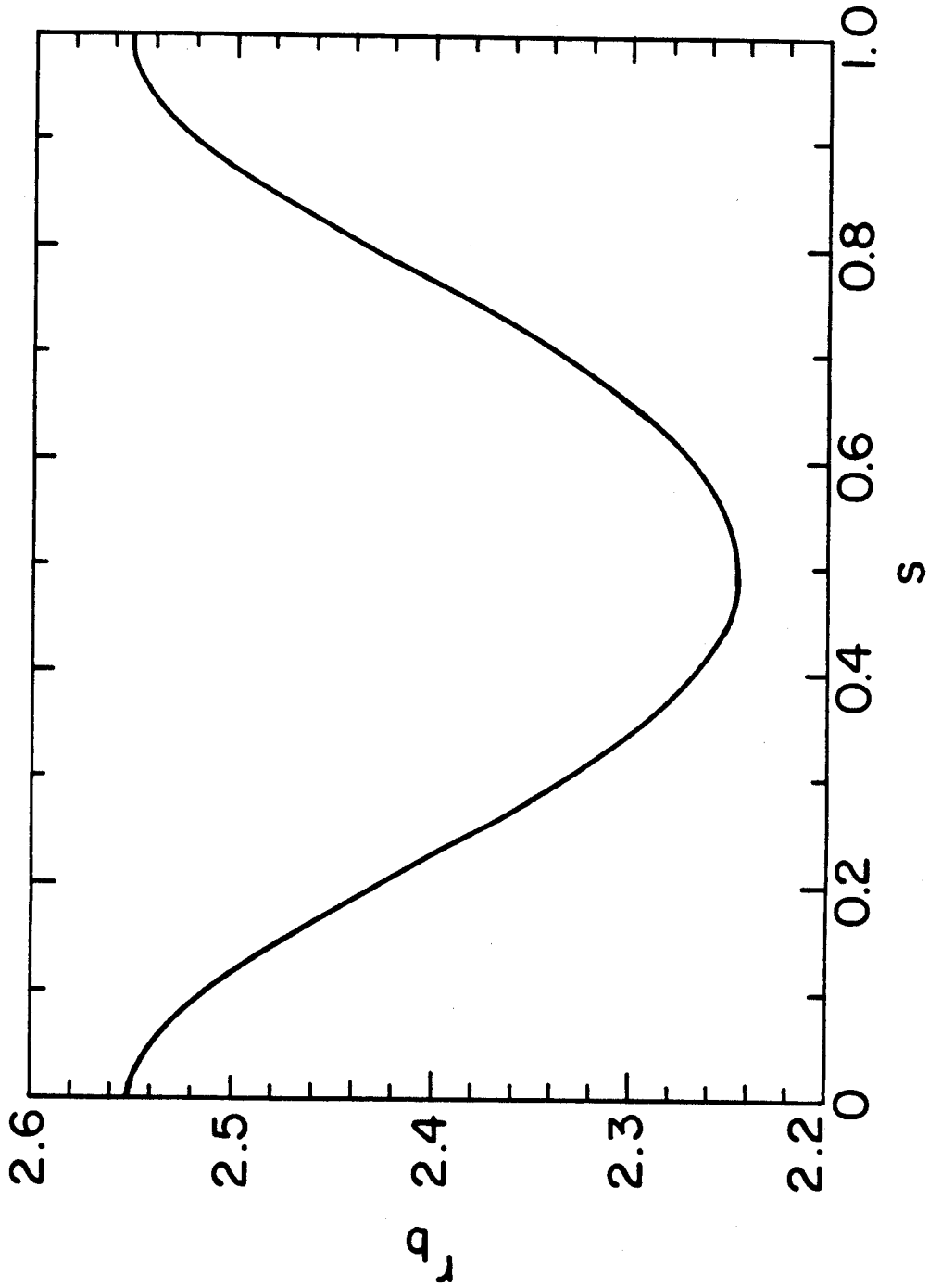

Figure 3

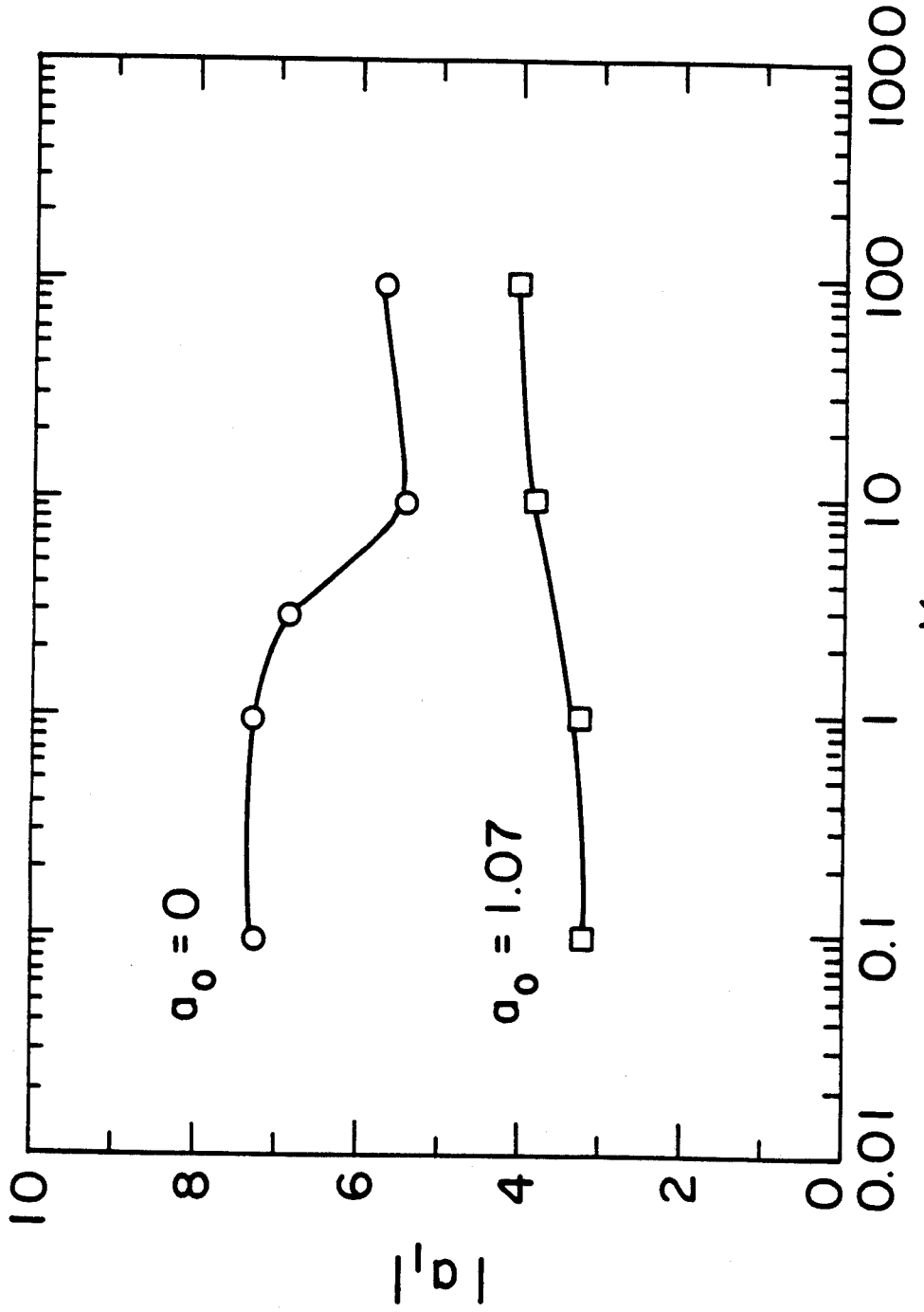

Figure 4

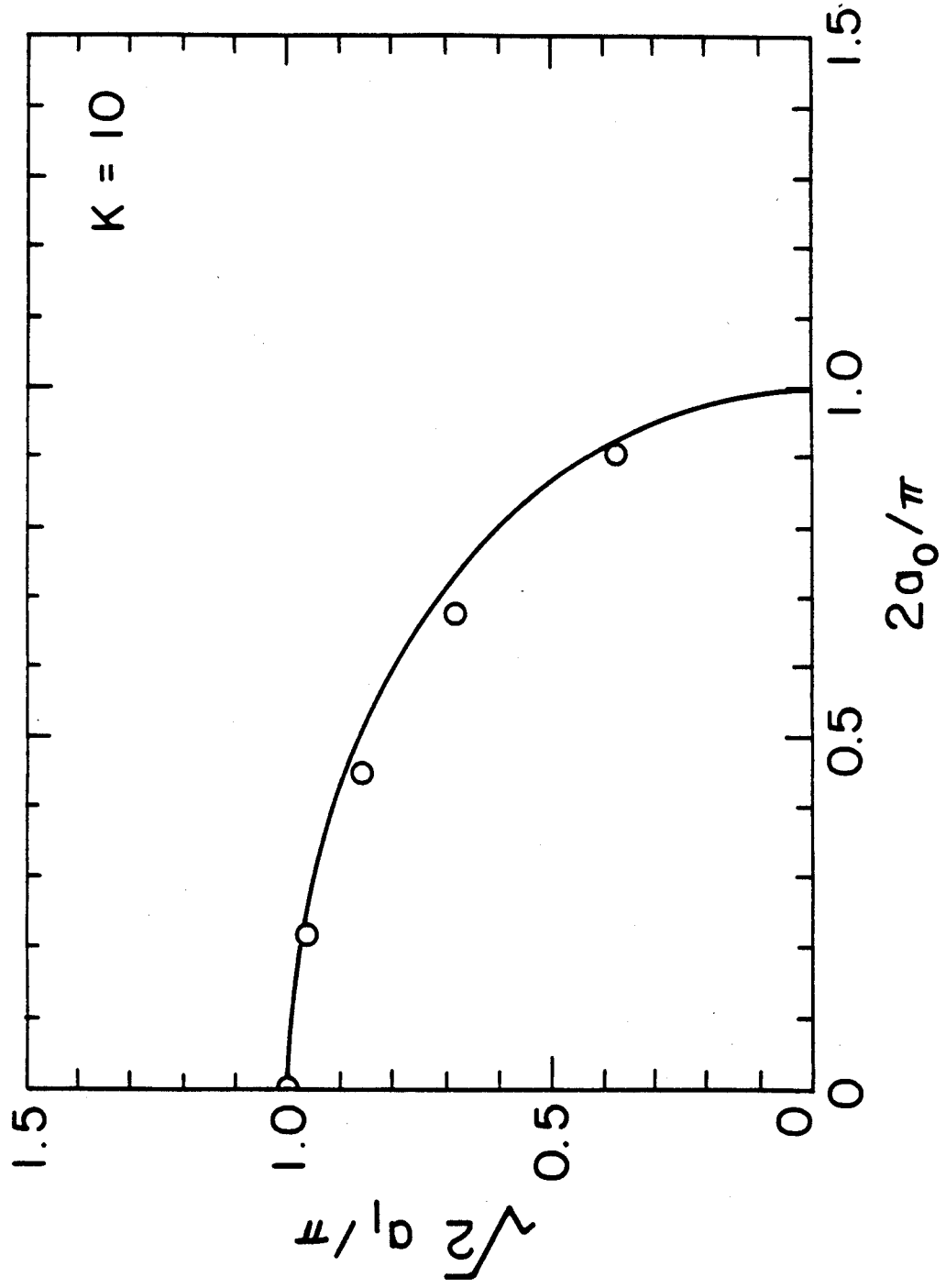

Figure 5